TRANSVERSE BEAM SIZE MEASUREMENT

G. Trad*, E. Bravin, B. Dehning, A. Goldblatt, F. Roncarolo, M. Sapinski, D. Vilsmeier
CERN, Geneva, Switzerland

Abstract

During the CERN long shutdown (LS1), most of the profile monitors in the LHC went through a consolidation or refurbishment programme to cope with the increase of the machine top energy to 6.5 (and later 7 TeV). In fact the resulting adiabatic reduction of the transverse geometric beam emittance combined with the increased brightness delivered by the injectors will bring most of the beam size monitors close or even beyond their resolution limits. In this paper we will summarize the upgrades/improvements carried out on the Wire Scanners (WS), Beam Gas Ionization (BGI) and the Synchrotron Radiation (BSRT) monitors, focusing on the expected performances and limits of the beam size measurements at top energy.

WIRE SCANNERS

Wire scanners are the reference devices for transverse beam size and emittance measurements in the LHC. They are also used for calibrating other instruments, such as the BGI and BSR monitors. The WS working principle, shown in Fig.1, consists of a thin carbon wire moved across the beam at the speed of about 1 m/s; the radiation produced by the interaction of the protons with the wire is observed by means of downstream scintillators coupled to Photo Multiplier Tubes (PMT). This charge deposition is proportional to the local density of the beam and is used to measure a beam density profile.
The LHC is equipped with eight WS systems. Four are kept operational (one per plane per beam) while four spares can be connected remotely without interventions in the machine.

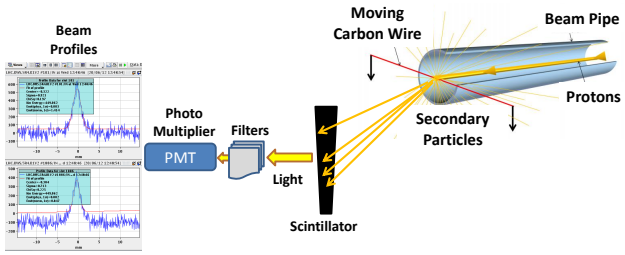

Figure 1: Schematics of the WS chain, presenting its working principle.

During LS1, mainly maintenance tasks were carried out on the WS.

On the hardware level, after evidence of aging due to the sublimation process, the wires were replaced by the same type of Carbon wires (diameter: 30 µm). In addition, following the failure of one of the systems after 10200 scans, related to bellow vacuum leaks causing a 24 h stop of the LHC operation, the old WS bellows designed to withstand about 10000 scans were replaced by a new design of a higher lifetime (40000 cycles). The number of scans per device are continuously logged and monitored through automated software reports.

The low level software of the WS also went into a consolidation program, mostly aiming to avoid dangerous situations that caused the wire breakage during Run 1 operation: the crash of the FESA server driving the wire movement following operator requests of scanning both beams contemporaneously lead to wires remaining stuck in the “IN" position with circulating beam. Furthermore, the WS user application was completely renovated , getting simpler and more powerful. The GUI will :

- allow an automatic selection for all the bunches circulating in the machine,
- allow automatic scans for both planes and both beams,
- allow repetitive scans per beam,
- feature one gain setting combining the PMT gain and the light Neutral Density (ND) filters,
- feature different fit options on users request (fitting only the bunch core or including tails),
- allow importing custom machine optics for the emittance calculations.

Moreover, studies showed a working point (PMT gain, ND filters) dependence on the measured beam size and intensity. Therefore, a new PMT is under test to mitigate measurements error due to the saturation effect. The option of a particle shielding is also investigated to solve possible non-linearity due to parasitic signal generated in the PMT. Beam studies in the coming machine development time will be needed to study the PMT saturation and implement a corresponding software warning to alert the user.

Following the 2013 beam-induced quench tests with 4 TeV protons, it was found that the maximum intensity limits measurable by the WS is defined by the Carbon wire breakage due to sublimation and not by the beam dump due to downstream BLM interlocks set to minimize the possibility of a superconducting magnet quench. The wire damage is not immediate above the new defined thresholds but scanning such high intensity beams would speed up the wire deterioration. Table 1 presents the found threshold for both beams at injection and 6.5 TeV for two beam emittances. To be noted that the different thresholds per beam and per plane is due to the optical function β value at the scanner location, hence eventual change of optics in IR4 would imply the modification of these thresholds.

* georges.trad@cern.ch

		BEAM 1		BEAM 2	
	ε (μm)	H	V	H	V
450 GeV	2	164	118	204	106
	3.5	217	156	269	141
7 TeV	2	53.1	51.5	51.6	26.9
	3.5	70.3	68.1	68.2	35.6

Table 1: Maximum beam intensity limits for WS measurements (in 10^{11} protons).

BEAM-GAS IONIZATION MONITOR

The Beam Gas Ionization monitors (BGI) are conceived to infer the LHC beam size from the measurement of the electrons distribution produced by the ionization of Neon gas injected into the vacuum chamber. The schematics in Fig.2 show the working principle of this monitor where the charged beam passes between two ceramic electrodes with a potential difference of 4 KV, over a distance of 85 mm. This potential brings the produced electrons to a Micro-Channel Plate (MCP), where the signal is amplified, before reaching a phosphor screen producing a photon distribution imaged by a complex optical system on a CCD intensified camera. In order to minimize the transverse spread of the electrons, external magnetic field of 0.2 T, directed along electric field lines, is applied.

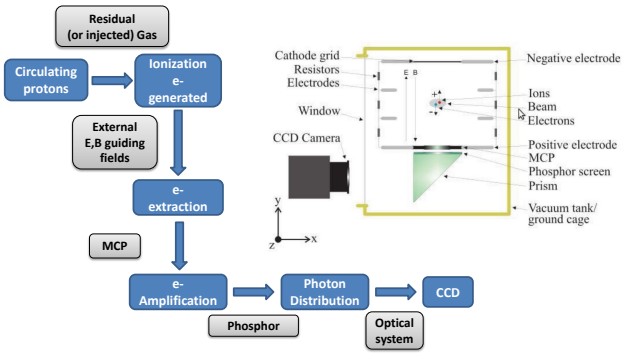

Figure 2: Schematics of the BGI chain, presenting its working principle.

The BGI monitors went through a maintenance program during LS1. On the hardware level, after clear signs of aging, the MCP and the adjacent phosphor screens where replaced by new ones of the same type. In order to avoid radiation damage to the CCD, a new radiation hard assembly is installed, where the camera chip is relocated in a separate shielded box provided by the manufacturer. Finally, in vacuum temperature probes were installed on two out of four monitors to study eventual beam induced heating issues in the detector.

Moreover, extensive simulations targeted the performance of the instrument and it was found that the electrons liberated in the ionization process strongly interact with the beam charges, affecting electron trajectories and the overall beam profile. The simulated profile broadening was more pronounced in the case of the expected 50 ns beam parameters, as shown in Fig.3, where the resulting beam profile is not gaussian anymore, but highly dominated by the space charge effect. The same simulations predict for the expected 25 ns beam parameters a smaller broadening than 7 TeV 50 ns beams mainly due to the reduced bunch charge and the larger emittances expected. However, this will not allow correct direct measurements of proton beams. It is important to note that the correction algorithm under development depends on the bunch length and intensity, so for the moment it is not foreseen to be done on-line. However, for the ion beams, the space charge effect is negligible and BGI shall be functional.

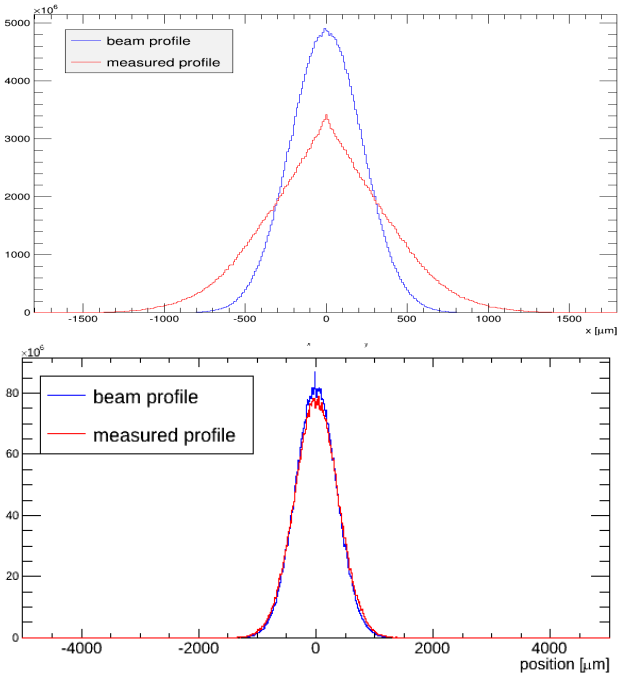

Figure 3: Profile broadening due to space charge effects, for protons (top) and ions (bottom), at flattop energy.

After LS1, for protons, the BGI will continue providing a beam size measurement resulting from the integration of the signal from the whole beam over many turns (10-100 ms integration time). On the other hand, due to the higher output signals from ions beams, a bunch-by-bunch measurement could be implemented exploiting the 50 ns gating possibilities of the camera. In case the software infrastructure will be available, these studies will take place in machine development periods.

SYNCHROTRON LIGHT MONITOR

The BSRT monitor images the synchrotron light generated by beam particles traversing a dedicated superconducting undulator and a D3 type dipole located in IR4. From the LHC injection energy (450 GeV) to about 1.5 TeV, the radiation generated by the undulator is in the visible

range, and shifts to the X-rays along the energy ramp. From 1.2 TeV onward the dominant component of the visible SR is emitted by particles traversing the D3.
At a distance of 26 m from the D3 entrance, the protons are sufficiently separated from the photons to provide room for a mirror that extracts the light, directing it downward through a fused-silica view port to an imaging optic system in a shielded enclave below the beam line.

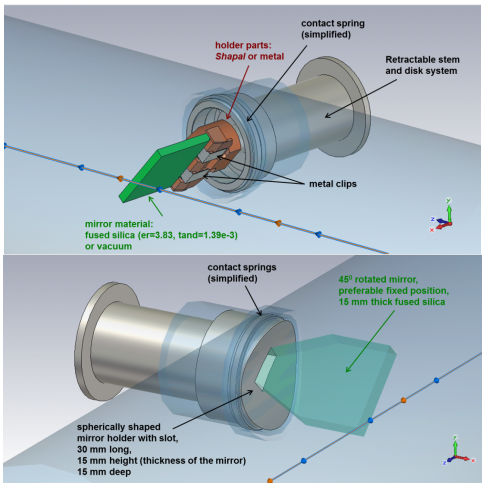

Figure 4: OLD (top) vs NEW (bottom) BSRT extraction mirror and its holder.

During the LHC operation in Run 1, the overall performance of the SR imaging system was dominated by the gradual deterioration and heating of the extraction mirror that lead to its mechanical failure. As pointed out by the available temperature probes, a strong correlation was found between the mirror support heating and the longitudinal bunch length, shape and the total beam intensity. These observations trace back the heating origin to electromagnetic coupling between the beam and the structure. Therefore, with the constraint of keeping the light extraction tank unchanged, a new design of the extraction mirror and its holder was implemented as shown in Fig.4. A longer glass bulk, dielectric coated mirror is inserted through a slit in the beam-pipe replacing the original silicon bulk mirror dielectric coated one. This geometric modification hides the mirror holder and shaft completely, showing no dominant resonance effects in the wake impedance simulation, thus avoiding the need for resonance damping materials, e.g. ferrites. It is worth noting that a very good agreement (within 10%) was found between the EM simulations and laboratory measurements based on the stretched wire method using a spare BSRT tank.

In addition to the in-vacuum temperature probes monitoring eventual heating in the structure, a movable Shack-Hartman mask will be installed just after the view port to monitor the quality of the light extraction mirror. This light-destructive measurement consists of an opaque plate with a regular holes matrix (1 mm diameter each) to be inserted just after the extraction mirror; its projection, illuminated by the SR, will be observed by a CCD camera on a screen located several meters after the mask. Each hole samples a small area of the mirror, and in case of a flat "non-deformed" mirror, a regular spacing pattern is measured on the camera; contrarily, if the extraction mirror is deformed by the heating, by analysing the arrangement of the matrix projection and by calculating the separations between the holes, the distortion of the mirror can be calculated and its surface can be reconstructed.

In addition, only for Beam 1, a new external alignment line was installed, consisting in a modified $BTVSI$ tank replacing the $BSRTA$ (periscope) to allow both imaging calibration and alignment via the same optical line that includes the extraction mirror as well. Therefore the bulky 26 m calibration line will be removed freeing half of the optical bench.

The extracted visible SR light is shared on the optical table among the imaging system measuring the transverse profile of the beam, the Abort Gap Monitor (AGM) and the Longitudinal Density Monitor (LDM) used to characterize the longitudinal distributions of the LHC beam. The AGM verifies continuously that there are no particles within the rise time gap (3 ms) of the dump extraction kicker (MKD); Particles in this gap would indeed not receive the proper kick when the dump system is fired and would damage machine components. In order to not compromise the stability and reliability of this monitor , needed for machine protection, a light wedged splitter was installed immediately after the extraction mirror to completely decouple longitudinal and transverse diagnostics.

Extensive simulations were carried out targeting the imaging system and dedicated tools were developed to assess its performance. With the increasing LHC flat top energy to 6.5 TeV, due to the adiabatic emittance shrinking, the beam size at the SR source will be reduced by 30% getting smaller than the monitor resolution itself. Hence, at high energy, to reduce the Line Spread Function (LSF) of the BSRT, dominated mostly by diffraction smearing, the working wavelength had to be shifted from 400 nm to 250 nm. Clear benefits in terms of resolution are shown in Fig.5. Consequently, as shown in Fig.8 interchangeable focusing lenses will be used to monitor red light at injection energy (green lens A) and near UV at flattop (blue lens B).

However, due to the inevitable small source size, reaching the required precision on the emittance measurement ($<$ 10%) remains a difficult task. The measured beam size by SR imaging corresponds to the real proton beam size broadened by diffraction and lens aberrations and eventual distorted surfaces causing the wavefront deformation; hence the beam size from the BSRT is obtained by subtracting in quadrature a correction factor σ_{corr} from the measured

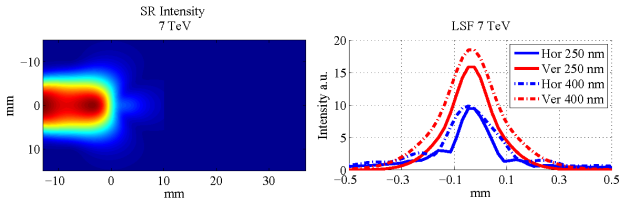

Figure 5: Deposited SR intensity emitted by a zero emittance beam at 7 TeV on the BSRT extraction mirror (left) and a comparison of its image (Line Spread Function) through the BSRT lens system for 250 nm vs 400 nm.

value:

$$\sigma_{beam_{BSRT}} = \sqrt{\sigma^2_{meas_{BSRT}} - \sigma^2_{corr}} \tag{1}$$

where the correction factor is retrieved by calibrating the BSRT measurements to the WS measurements:

$$\sigma^2_{corr} = \sigma^2_{meas_{BSRT}} - \beta_{ratio} \cdot \sigma^2_{meas_{WS}} \tag{2}$$

with β_{ratio} being the ratio of the β at the D3 and the WS location. Due to the relative errors on the measurements in the WS, the BSRT and the knowledge of the β_{ratio} respectively:$\epsilon_{\sigma_{meas_{WS}}}$, $\epsilon_{\sigma_{beam_{BSRT}}}$ and $\epsilon_{\beta_{ratio}}$, the resulting relative error on the beam size determination using the BSRT can be expressed by:

$$\epsilon_{\sigma_{beam_{BSRT}}} = \frac{1}{2}\left\{8\epsilon^2_{\sigma_{meas_{BSRT}}} \cdot \left(1 + \left(\frac{\sigma_{corr}}{\sigma_{real}}\right)^2\right)^2 + \epsilon^2_{\beta_{ratio}} + 4 \cdot \epsilon^2_{\sigma_{meas_{WS}}}\right\}^{0.5} \tag{3}$$

The amplification factor in the error expression, $\frac{\sigma_{corr}}{\sigma_{real}}$ can be reduced by increasing the beam size at the dipole D3 by increasing β_{BSRT}. Figure 6 shows the effect of increasing the beta function on the overall BSRT beam size determination accuracy, for an optimistic situation where $\sigma_{corr} = 250\,\mu m$, $\epsilon_{\sigma_{meas_{WS}}} = 1\%$, $\epsilon_{\sigma_{beam_{BSRT}}} = 1\%$ and $\epsilon_{\beta_{ratio}} = 2\%$.
The two vertical black dashed lines in Fig.6 represent the nominal minimum value of $\beta_{BSRT} = 127$ m (Beam 2 Horizontal plane) and the increased value proposed in the modified IR4 optics $\beta_{BSRT} = 200$ m (feasibility of the optics change is still under investigation).

To overcome this intrinsic limitation of the visible SR imaging, a new beam size monitor, visible SR double-slit Interferometry (SRI), will be tested and implemented in the free space on the optical table for Beam 1. This monitor is a wavefront-division type two-beam interferometer using polarized quasi-monochromatic SR light.

The method, first applied by Michelson for measuring angular dimensions of stars, allows the determination of the size of a spatially incoherent source by measuring the spatial distribution of the degree of coherence after

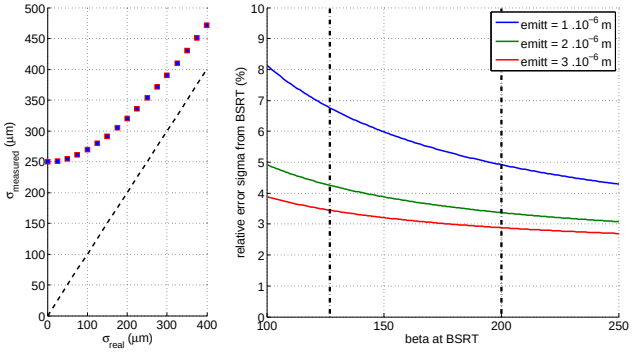

Figure 6: Given a σ_{corr} =250 µm, the broadening effect is shown in the left plot where the effective beam size measured (red) is compared to the real beam size (dashed). At the varying bsrt beam size measurement error function of beta.

propagation and is based on the Van Cittert–Zernike (VCZ) theorem, which states that there is a Fourier transform relation between the intensity distribution of an incoherent object and the complex degree of coherence measured in the far field. Its application to synchrotron radiation beam profiling was first proposed and demonstrated by Mitsuhashi as shown in Fig.7 and nowadays is widely diffused in most of the SR storage rings.

A feasibility study of the SRI for the LHC beams was carried out starting from the validity of VCZ: its application is not straightforward due to the small beam size and divergence with respect to the big opening light cone angle. Such beam parameters result in a big coherence area of the propagated wavefront for visible wavelengths. Moreover, due to the big bending radius of D3 ($\rho \sim 6\,Km$), an important component of the fringes visibility reduction is not determined by the beam size but by the incoherent depth of field. In addition, since the main part of the visible SR intercepted by the extraction mirror is emitted in the rising magnetic edge of the D3, strong intensity imbalance can be found on the slits (horizontal separation) that further decreases the fringes visibility. All the aforementioned phenomenas and the distorted surfaces of the mirrors and the lens aberrations lead to the development of a dedicated simulation suite that realistically describes the SRI optical system and its source. A resulting mapping of the measurable fringe visibility to the beam size is presented in Fig.7.

With the fully automated double slit (slit separation and slit width) system under development, interferometry tests are planned to be done at injection energy and at flattop, thus measuring beam sizes ranging from 150 μm to 1.3 mm, in both planes, individually or simultaneously. However, retracting completely the slits will allow to perform SR imaging using the high frame rate intensified sCMOS camera, which has been chosen for the interferometer line. With a frame rate close to 1000 fps, beam tomography could be tested as well for Beam 1.

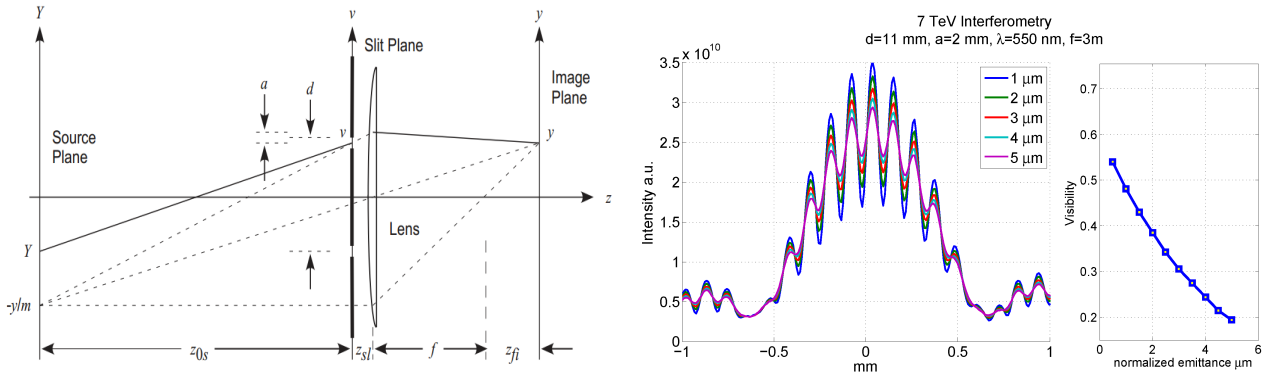

Figure 7: Interferometry working principle (left) and visibility mapped to beam size as a result of the simulations (right).

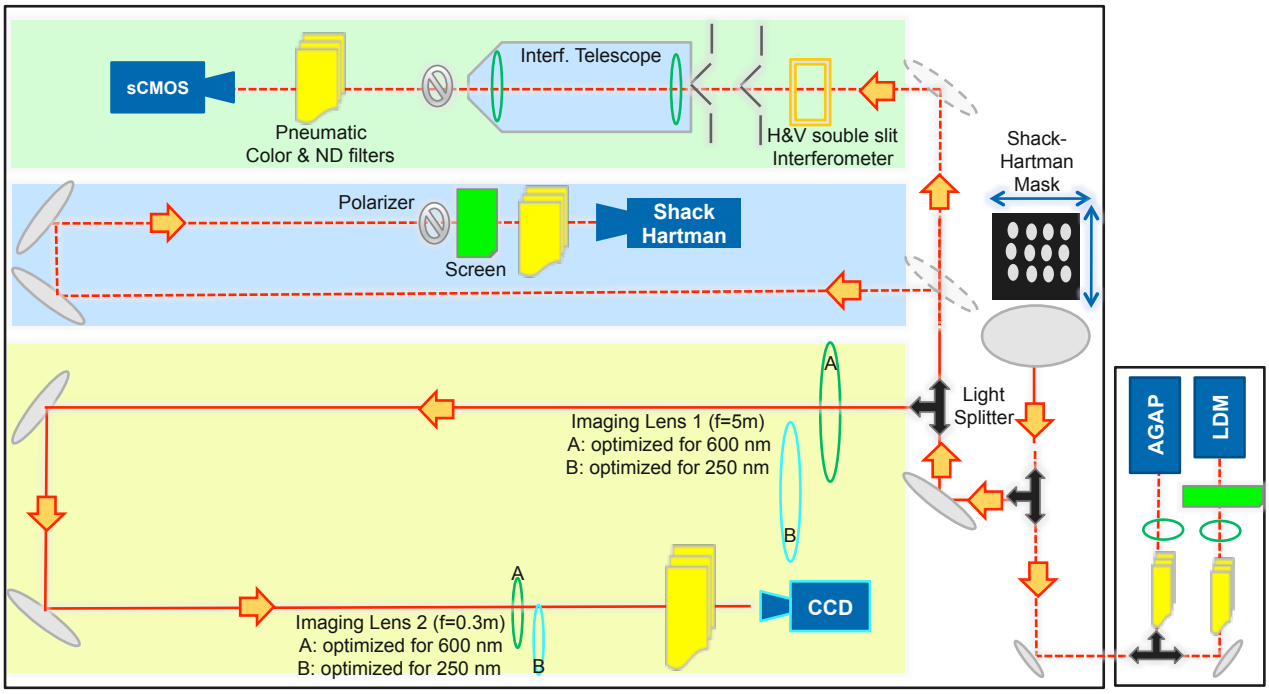

Figure 8: Beam 1 optical table layout after LS1.

Finally, the low level control server will be upgraded, mainly for consolidation of the automated feedbacks and for coping with the HW changes on the optical table equipment (e.g. pneumatic filter system instead of motorized wheels and double slits control). Operationally, the BSRT imaging system will continue providing beam size measurement at 450 GeV and 6.5 TeV at $\sim 25Hz$, thus measuring the full beam in ~20 minutes. Test are planned for measurements through the energy ramp, during MD.

CONCLUSIONS

An overview of the status of the main beam size monitors in the LHC pointed out the consolidation, maintenance and upgrades tasks carried out during LS1. Important modification, both at hardware and software level, were presented, giving a summary of the expected performance with the new beam conditions expected in LHC Run 2.

REFERENCES

[1] T. Mitsuhashi, Measurement of small transverse beam size using interferometry, Proc. of DIPAC'2001, Grenoble (France).

[2] J. Emery et al., PERFORMANCE ASSESSMENT OF WIRE-SCANNERS AT CERN, TUPF03, IBIC2013, Oxford (UK).

[3] F. Roncarolo et al., WHAT YOU GET? TRANSVERSE AND LONGITUDINAL DISTRIBUTIONS, LHC Beam Operation workshop, Evian 2012.

[4] A. Goldblatt et al., A NOVEL APPROACH TO SYNCHROTRON RADIATION SIMULATION, THPME177, IPAC2014, Dresden (Germany).

[5] F. Roncarolo et al., ELECTROMAGNETIC COUPLING BETWEEN HIGH INTENSITY LHC BEAMS AND THE SYNCHROTRON RADIATION MONITOR LIGHT EXTRACTION SYSTEM, TUPFI063, IPAC2013, Shanghai (China).

[6] G. TRAD et al., A NOVEL APPROACH TO SYNCHROTRON RADIATION SIMULATION, THPME177, IPAC2014, Dresden (Germany).

[7] G. TRAD et al., Optics modifications implications on beam size measurements in LHC IR4, LHC Beam Operation Committee LS1 LBOC meeting No 17.

[8] M. Sapinski et al., Status of Beam Gas Ionization Monitor, LHC Beam Operation Committee LS1 LBOC meeting, 10 July 2012.

[9] M. Sapinski et al., The First Experience with LHC Beam Gas Ionization Monitor, THPB61, IBIC2012, Tsukuba (Japan).

[10] M. Patecki et al., Analysis of LHC Beam Gas Ionization monitor data and simulation of the Electron transport in the detector, CERN-THESIS-2013-155.